Iranian Journal of Basic Medical Sciences
ijbms.mums.ac.ir

Combined cold atmospheric plasma and vemurafenib suppress MITF–P21 signaling and MMP-driven metastasis in cutaneous melanoma

Zahra Yazdani [1, 2], Mansooreh Mirzaei [3], Sadegh Fattahi [4], Farshad Sohbatzadeh [5], Saeid Abediankenari [6], Arefe Mousavi [7], Fatemeh Mirbabaei [7], Zeinab Rostami [1, 2], Monireh Golpour [8], Alireza Rafiei [1]*

[1] Department of Immunology, Molecular and Cell Biology Research Center, School of Medicine, Mazandaran University of Medical Sciences, Sari, Iran
[2] Students Research Committee, Mazandaran University of Medical Sciences, Sari, Iran
[3] Department of Anatomy, School of Medicine, Mazandaran University of Medical Sciences, Sari, Iran
[4] North Research Center, Pasteur Institute of Iran, Amol, Iran
[5] Department of Atomic and Molecular Physics, Faculty of Science, University of Mazandaran, Babolsar, Iran
[6] Immunogenetics Research Center, Department of Immunology, Faculty of Medicine, Mazandaran University of Medical Sciences, Sari, Iran
[7] Department of Basic Sciences, Sari Agricultural Sciences and Natural Resources University, Sari, Iran
[8] Cancer Research Center, Health Research Institute, Babol University of Medical Sciences, Babol, Iran

ARTICLE INFO

Article type:
Original

Article history:
Received: May 2, 2026
Accepted: Jun 19, 2026

Keywords:
Animal
In vitro
In vivo
Melanoma
Matrix metalloproteinases-
Models
Plasma gases
Vemurafenib

ABSTRACT

Objective(s): This study investigated the anti-tumor efficacy of combined cold atmospheric plasma (CAP) and Vemurafenib (VEM) treatment (CAP plus VEM) in cutaneous melanoma, focusing on the MITF–P21 axis and MMP-driven metastasis.

Materials and Methods: The therapeutic effects of CAP and VEM were evaluated using *in vitro* and *in vivo* models. B16-F10 melanoma and L929 fibroblast cell lines were used to assess long-term cell proliferation and migration using clonogenic and wound-healing assays. *In vivo*, melanoma tumors were induced in C57BL/6 mice followed by treatment with CAP, VEM, or CAP plus VEM. Tumor tissues and major organs were collected for histopathological evaluation and molecular analysis. Gene expression levels of MITF, P21, MMP-2, and MMP-9 were quantified by qRT-PCR in both experimental settings.

Results: CAP and VEM significantly inhibited melanoma cell proliferation and migration, with the CAP plus VEM showing the most pronounced effect. In vitro, all treatments markedly down-regulated *MITF*, *P21*, and *MMP-2* gene expression ($P<0.0001$). Histopathological analysis revealed extensive tumor necrosis, reduced cellularity, and improved tissue architecture in the CAP plus VEM group, accompanied by fewer metastatic alterations in major organs. qRT-PCR of tumor tissues confirmed significant down-regulation of *MMP-2* and *MMP-9* after CAP, VEM, and especially the CAP plus VEM group ($P<0.0001$). The modest *in vivo* changes in *MITF* and *P21* may reflect microenvironmental influences.

Conclusion: The CAP plus VEM enhances anti-tumor efficacy and suppresses metastasis-related pathways in melanoma, both *in vitro* and *in vivo*. This suggests a promising complementary therapeutic strategy.

▶ Please cite this article as:
Yazdani Z, Mirzaei M, Fattahi S, Sohbatzadeh F, Abediankenari S, Mousavi A, Mirbabaei F, Rostami Z, Golpour M, Rafiei AR. Combined cold atmospheric plasma and vemurafenib suppress MITF–P21 signaling and MMP-driven metastasis in cutaneous melanoma. Iran J Basic Med Sci 2026; 29:

Introduction

Cutaneous melanoma is an aggressive skin cancer, accounting for 331,722 new cases and 58,667 deaths in 2022 (1). Current therapeutic options for this cancer face challenges such as long-term side effects, treatment resistance, increased toxicity to normal cells, and high costs (2-6). Recently, combination therapies have been explored in various experimental and clinical studies. It has been shown that combining anticancer agents is more effective than monotherapy. This is because it targets key pathways synergistically or additively. Therefore, it can overcome cancer cell resistance and activate anti-cancer pathways (7). While combination therapies have the potential to improve treatment outcomes, they may also be associated with additional adverse effects, such as fever, and their therapeutic advantage over monotherapy is not always guaranteed (7, 8). Therefore, the selection of therapeutic agents, their mechanisms of action, and the appropriate dosage regimens should be carefully defined when developing combination treatment strategies.

***Corresponding author:** Alireza Rafiei. Department of Immunology, Molecular and Cell Biology Research Center, School of Medicine, Mazandaran University of Medical Sciences, KM 18 Khazarabad Road, Khazar Sq, Sari, Iran. Tel: +98-113-3543614, Fax: +98-113-354-3087, Email: rafiei1710@gmail.com

Vemurafenib (VEM) is a selective small-molecule inhibitor of the B-Raf proto-oncogene (BRAF) kinase that has been approved by the U.S. Food and Drug Administration (FDA) for the treatment of cutaneous melanoma. Despite its efficacy, issues such as resistance and systemic toxicity have been reported. Several studies have shown that combination therapy with VEM and other drugs may decrease its challenges (9-11). Therefore, identifying effective and biologically rational combination strategies remains an important unmet clinical need.

Cold atmospheric plasma (CAP) is a promising new approach in oncology and regenerative medicine. As an ionized gas rich in reactive oxygen and nitrogen species (RONS), it has been widely investigated as a therapeutic modality against various cancers. Studies also indicate that combining CAP with other anti-cancer treatments may enhance overall therapeutic effects (12-16). However, several challenges remain before such approaches can be effectively translated into clinical practice. In particular, the therapeutic agents involved, their mechanisms of action, and the applied dosage regimens must be carefully defined to avoid antagonistic interactions and to maximize therapeutic efficacy (17-19).

The microphthalmia-associated transcription factor (MITF) and cyclin-dependent kinase inhibitor 1 (P21) contribute to uncontrolled cell proliferation in melanoma. Therefore, targeting this pathway could provide a novel and effective strategy for therapeutic development. The MITF-P21 signaling cascade not only governs cell cycle progression but also influences phenotypic switching in melanoma (20-22). Dysregulation of this axis may promote metastatic behavior, in which matrix metalloproteinases-2 and -9 (MMP-2 and MMP-9) act as key mediators. MMPs are a family of zinc-dependent endopeptidases. They have the potential to degrade basement membrane and extracellular matrix components, thereby facilitating cell migration (23-25). Among this family, the gelatinases MMP-2 (72 kDa type IV collagenase) and MMP-9 (92 kDa type IV collagenase) are closely linked to malignant progression due to their ability to degrade type IV, V, VII, and X collagens, fibronectin, and gelatin within basement membranes (25). Therefore, any agent that reduces MMP-2 and MMP-9 gene expression may reduce cancer progression and metastasis.

Given the potential advantages of combination therapy and the emerging anti-cancer properties of CAP, investigating the interaction between CAP treatment and BRAF inhibition may provide additional insights into melanoma therapy. Therefore, the present study aimed to assess the combined effects of CAP and VEM (CAP plus VEM) on melanoma suppression. *In vitro*, the clonogenic ability and wound-healing capacity of cancer cells were evaluated. Additionally, *in vivo* histopathological analysis of tumors and organs with metastatic potential was performed. Both experimental phases emphasized their impact on the MITF–P21 axis and MMP-mediated metastasis.

Materials and Methods

Materials and Reagents

Vemurafenib (VEM; ≥98% purity) was purchased from a commercial supplier and dissolved in dimethyl sulfoxide (DMSO) to prepare a 10 mM stock solution. The stock was aliquoted and stored at −80 °C until use. RPMI-1640 culture medium, fetal bovine serum (FBS), penicillin–streptomycin, and trypsin–EDTA were obtained from Biosera (France). RNA extraction and cDNA synthesis kits were purchased from Favourgen (Taiwan) and Parstous (Iran). Quantitative TaqMan qRT-PCR reagents were obtained from Qiagen (Hilden, Germany), while quantitative SYBR Green qRT-PCR mastermix was obtained from AMPLIQON (Denmark). All other chemicals and reagents were of analytical grade and sourced from Sigma-Aldrich (St. Louis, MO, USA), unless otherwise stated.

Cell culture

The murine melanoma cell line B16-F10 and the normal murine fibroblast cell line L929 were procured from the Pasteur Institute of Iran (Tehran, Iran). Both cell lines were maintained in RPMI-1640 medium supplemented with 10% FBS and 1% penicillin–streptomycin. Cells were cultured at 37 °C in a humidified atmosphere containing 5% CO_2. The culture medium was refreshed every three days, and cells were passaged at 70–80% confluence using 0.25% trypsin–EDTA.

Clonogenic assay

To assess the long-term effects of each treatment on cancer progression, a clonogenic assay was performed. Briefly, B16-F10 and L929 cells were seeded in 24-well culture plates at a density of 1000 cells per well. Following an overnight attachment period, the cells were exposed to the following treatments: CAP for 70 sec, 20 µM of VEM, or CAP plus VEM. These cytotoxicity and mechanistic analyses were investigated in another work (in press). Details regarding the CAP device, exposure parameters, and treatment conditions have been reported in our previously published articles (13, 14, 26, 27). In summary, CAP was produced using an argon-driven plasma jet device. During treatment, the jet nozzle was positioned 3 cm above the culture medium surface, and cells were exposed to CAP generated at 14 kV for 70 sec. These treatment parameters were selected based on our previously optimized protocol. The physicochemical characterization of the CAP device, including the generation of reactive species under these operating conditions, was evaluated in another work (in press). After 7 and 14 days of treatment, the cells were kept at 37 °C in a humidified atmosphere containing 5% CO_2 to allow colony formation. During this period, the culture medium was replaced with fresh medium every three days. After incubation, the medium was removed. Colonies were rinsed with Phosphate-buffered saline (PBS), fixed, and stained with glutaraldehyde–crystal violet solution for 30 min, washed with water, and air-dried at room temperature (28).

Wound healing assay

Cell migration was assessed using a wound healing (scratch) assay. B16-F10 melanoma and L929 fibroblast cells were seeded in 24-well plates and cultured at 37 °C with 5% CO_2 until reaching a confluent monolayer. A uniform cross-shaped scratch was created in the center of each well using a sterile 100-µl pipette tip. Cellular debris and detached cells were gently removed by washing twice with PBS. To minimize cell proliferation and allow selective assessment of cell migration, the culture medium was replaced with fresh medium supplemented with 1% FBS. Cells were subsequently exposed to CAP, VEM, or CAP plus VEM. Phase-contrast images of the wound area were taken at 0, 24, and 48 hr using an inverted microscope.

Animal model and treatment

Female C57BL/6 mice (6–8 weeks old) were used to establish the melanoma model. B16-F10 cells (8.5×10^5 cells in 100 µl PBS) were injected subcutaneously into

the right flank. Tumor progression was monitored daily until the tumor became palpable (7th day). The mice were randomized into four groups: untreated control, VEM, CAP, and CAP plus VEM treatments. CAP was administered under ketamine–xylazine anesthesia. The treatment was performed under conditions similar to those used for the cell experiments. The plasma jet nozzle was positioned 3 cm above the tumor surface, and tumors were exposed to CAP for 5 min. CAP treatment was applied once every five days throughout the experimental period. VEM was delivered by oral gavage at 70 mg/kg/day for five consecutive days each week. Mice were euthanized 14 days after the initial observation of the tumor. The study endpoint (TTE) was reached when animals met any of the predefined humane criteria, including a loss of more than 15% of initial body weight, reduced health status, or obvious disease-related symptoms. Finally, tumors and potential metastatic organs (liver, kidney, lung, brain) were harvested for molecular and histological analyses. All procedures were approved by the Research Ethics Committee of Mazandaran University of Medical Sciences (IR.MAZUMS.AEC.1402.079).

Histopathological analysis

Tumor and organ specimens were fixed in 10% neutral-buffered formalin for 48 hours. They were then dehydrated through a graded ethanol series, cleared in xylene, and embedded in paraffin. Sections of 4–5 µm thickness were prepared using a rotary microtome and stained with hematoxylin and eosin (H&E). The tumor sections were evaluated for necrosis, cellular atypia, mitotic index, and stromal alterations. Organ sections (liver, kidney, lung, brain) were examined for inflammatory changes, structural abnormalities, and potential treatment-related toxicity.

Analysis of gene expression

For the *in vitro* experiments, B16-F10 and L929 cells were seeded into 24-well culture plates at a density of 1.2×10^5 cells per well. After overnight incubation to allow adherence, cells were treated according to the experimental groups described above. Following 24 hr of exposure, cells were harvested by trypsinization. Finally, total RNA was extracted using a commercial RNA isolation kit following the manufacturer's protocol. For the *in vivo* study, approximately 50 mg of each snap-frozen tumor sample was homogenized and processed for RNA extraction using a commercial kit, following the manufacturer's instructions. For both *in vitro* and *in vivo* samples, 0.1 µg of purified RNA was reverse-transcribed into cDNA using a standard cDNA synthesis kit. Quantitative real-time PCR was performed using a stem-loop TaqMan assay for *MMP-2* and *MMP-9* (29, 30). The SYBR Green method was used to assess *P21* and *MITF* expression. Gene expression levels were analyzed using the StepOnePlus™ Real-Time PCR system (Applied Biosystems, Waltham, MA, USA). Thermal cycling was performed under the following conditions: an initial denaturation step at 95 °C for 15 min, followed by 45 amplification cycles consisting of denaturation at 95 °C for 15 sec and annealing/extension at 60 °C for 1 min. Quantitative real-time PCR data were analyzed using the comparative C_t ($2^{-\Delta\Delta Ct}$) method to determine relative gene expression levels. GAPDH and HPRT were used as internal reference genes for normalization. Primer sequences are listed in Table 1.

Table 1. Primer sequences used to investigate MITF–P21 signaling and MMP-mediated metastasis

Gene name	Accession number	Primers 5' ➔3'	Ref.
GAPDH	NM_001289726.1	Forward primer: TTGTCAAGCTCATTTCCTGGTATG Reverse primer: GTCGTATCCAGTGCTGCGACCGTATGGATGTGTC TGCGGCGTTTTATCATGCACTGGATACGACGGAG GCCATGTAG	27
MMP-2	NM_008610.3	Forward primer: CGACCACAACCAACTACGATGATG Reverse primer: GTCGTATCCAGTGCTGCGACCGTATGGATGTGTC TGCGGCGTTTTATCATGCACTGGATACGGCTGCC ACGAGGA	This study
MMP-9	NM_013599.5	Forward primer: CCCAAAGACCTGAAAACCTCCAAC Reverse primer: GTCGTATCCAGTGCTGCGACCGTATGGATGTGTC TGCGGCGTTTTATCATGCACTGGATACGACTCTC CCATCATCTG	This study
HPRT	NM_013556.2	Forward primer: GGGATTTGAATCACGTTTGTG Reverse primer: TTACTGGCAACATCAACAGG	26
MITF	NM_001113198.2	Forward primer: CAGAGAGTGAGTGCCCAGGTATG Reverse primer: TCAAGTTTCCAGAGACGGGTAACG	This study
P21	NM_007669.5	Forward primer: CCAGCCTGACAGATTTCTATCACTCC Reverse primer: CCTCCTGACCCACAGCAGAAGAG	This study

MITF: Microphthalmia-associated transcription factor; MMP: Matrix metalloproteinases

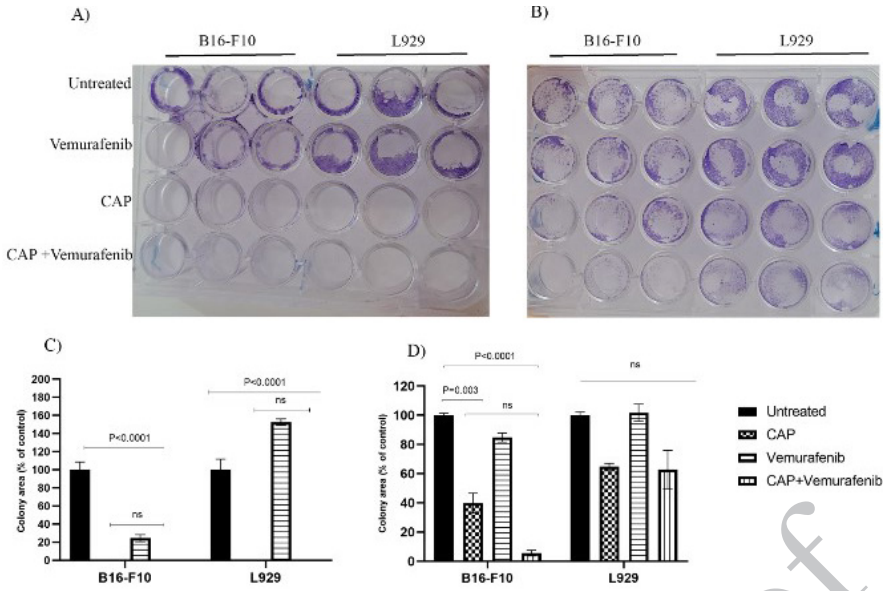

Figure 1. Effects of CAP, VEM, and CAP plus VEM on clonogenic survival of B16-F10 melanoma and L929 normal fibroblast cells
(A–B) Representative images of colony formation after 7 days (A) and 14 days (B) of incubation following treatment. (C–D) Quantification of total colony area after 7 days (C) and 14 days (D), normalized to untreated controls (set to 100%). Data are presented as mean±SEM from three independent experiments.
ns: not significant; CAP: Cold atmospheric plasma; VEM: Vemurafenib

Statistical analysis

Statistical analysis was performed using GraphPad Prism 8 and SPSS 22. *In vitro* experiments were performed in three independent biological replicates. Animal experiments were conducted in accordance with institutional guidelines for the care and use of laboratory animals and ethical principles, to minimize animal suffering and reduce the number of animals used. The minimum number of animals necessary to achieve a reliable statistical analysis was used in each experimental group. Data are presented as mean±SEM. Differences among multiple groups were analyzed using one-way analysis of variance (ANOVA) followed by the Tukey HSD post-hoc test. A significance level of $P<0.05$ was considered statistically significant. Effect sizes for ANOVA analyses were estimated using eta and omega squared (η^2, ω^2). Correlation analysis between gene expression levels was performed using Spearman's rank correlation coefficient based on ΔCt values obtained from qRT-PCR data. All correlation analyses were conducted using a two-tailed test, and *P*-values<0.05 were considered statistically significant. A full statistical summary table is shown in Supplementary Table 1.

Results

Effects of CAP plus VEM on clonogenic survival of melanoma cells

To evaluate the long-term effects of CAP, VEM, and their combination on clonogenic survival, a colony formation assay was performed in cancer and normal cells. Representative images of colonies after 7 days and 14 days of incubation are shown in Figures 1A and 1B, respectively. As shown in Figure 1C, treatment with CAP alone or CAP plus VEM significantly reduced the clonogenic area in both cancer and normal cells after 7 days compared with untreated controls ($P<0.0001$). After 14 days of incubation (Figure 1D), a partial recovery of clonogenic growth was observed in B16-F10 cells treated with CAP and VEM alone. However, CAP and CAP plus VEM treatments inhibited the clonogenic survival of these cells ($P=0.003$ and $P<0.0001$). In L929 cells, clonogenic growth was largely recovered after 14 days. Compared with the untreated group, none of the interventions had a significant effect on colony area.

CAP plus VEM inhibit melanoma cell migration in a wound-healing assay

In untreated B16-F10 cells, wound closure progressed over time. Cells showed substantial migration at 24 hr and near-complete closure by 48 hr, indicating high migratory potential. CAP treatment significantly delayed wound closure compared with the untreated group, and the scratched area remained partially open even after 48 hr. This suggests marked inhibition of cell migration. Additionally, treatment with VEM further reduced migratory activity compared with untreated cells. Notably, CAP plus VEM exerted the strongest inhibitory effect on cell migration. In this group, the wound area remained largely open at both 24 and 48 hr, with minimal cellular movement toward the scratched region. This indicates synergistic suppression of migratory capacity and metastatic potential in B16-F10 cells. In contrast, normal L929 cells exhibited lower sensitivity to the treatments. Despite modest inhibition by CAP plus VEM, L929 cells migrated more regularly and faster than B16-F10 cells. These findings indicate selective inhibition of melanoma cell migration, especially with CAP plus VEM treatment (Figure 2).

CAP plus VEM treatment attenuates tumor pathology and organ involvement

Histopathological examination of the tumor and major organs demonstrated clear treatment-dependent patterns consistent with the overall therapeutic response. In tumor sections, untreated mice exhibited densely packed malignant cells with pronounced nuclear pleomorphism, high mitotic activity, and marked vascular congestion. CAP or VEM monotherapy resulted in a noticeable decrease in tumor cellularity, accompanied by focal necrosis and partial restoration of tissue organization. CAP plus VEM

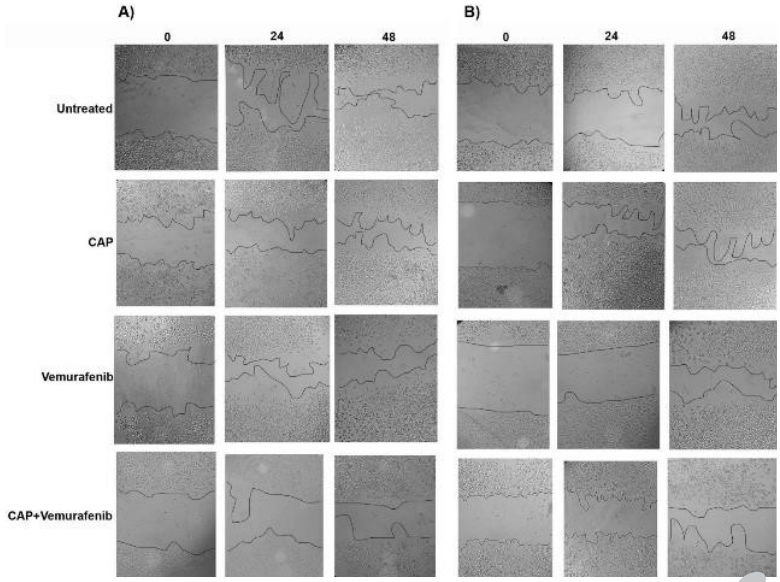

Figure 2. Effects of CAP, VEM, and their combination (CAP + VEM) on cell migration of:
(A) B16-F10 melanoma cells and (B) L929 fibroblast cells, as assessed by a wound-healing assay at 0, 24, and 48 hr. The combined treatment exhibited the greatest inhibitory effect on melanoma cell migration.
CAP: Cold atmospheric plasma; VEM: Vemurafenib

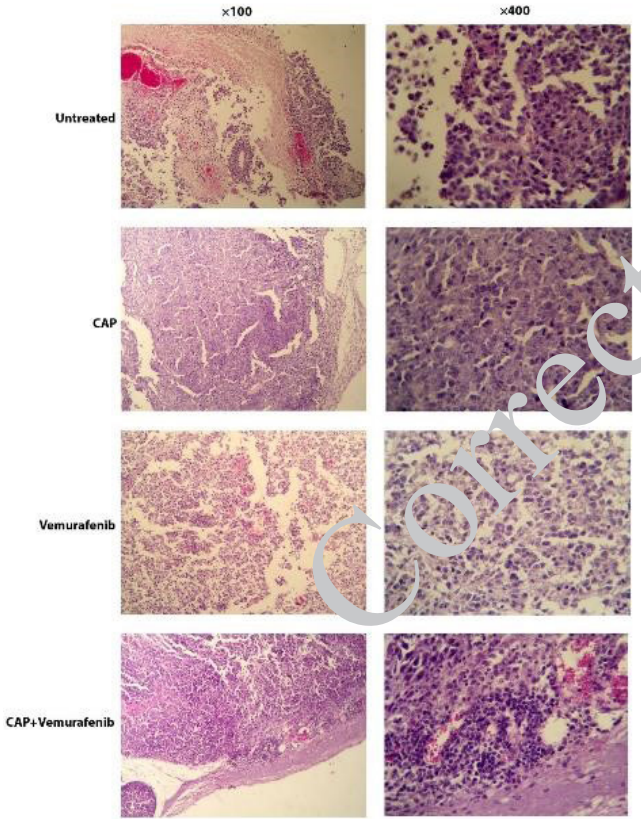

Figure 3. Histopathological evaluation of tumor tissues from C57BL/6 mice following CAP and vemurafenib treatment
Representative hematoxylin and eosin (H&E)–stained sections of tumor tissues from untreated, CAP-treated, vemurafenib-treated, and CAP plus VEM (CAP+Vemurafenib) groups are shown at low (×100) and high (×400) magnifications. Tumors from untreated mice exhibited dense cellularity, marked nuclear pleomorphism, and disorganized tissue architecture. CAP or Vemurafenib monotherapy reduced tumor cell density and partially restored tissue organization. Notably, the CAP+Vemurafenib treatment induced pronounced histopathological alterations. Extensive necrotic areas and marked disruption of tumor architecture were observed. In addition, the number of viable malignant cells was substantially reduced, indicating enhanced anti-tumor efficacy.
CAP: Cold atmospheric plasma; VEM: Vemurafenib

treatment induced the most pronounced histopathological alterations. This regimen resulted in widespread necrosis and extensive disruption of tumor architecture. Viable tumor areas were markedly reduced, and metastatic features within the surrounding stroma were substantially diminished. (Figure 3).

Lung tissue from untreated mice displayed diffuse septal thickening, inflammatory infiltrates, and multiple pigment-containing metastatic foci that disrupted alveolar spaces. CAP and VEM each attenuated these abnormalities, reducing inflammation and the number of melanin-positive cells. In the CAP plus VEM group, alveolar architecture was largely preserved, with minimal residual inflammation and only rare hyperchromatic cells, closely approximating normal lung structure (Figure 4).

In the liver, untreated samples showed hepatocyte disarray, sinusoidal dilation, inflammatory infiltrates, and hyperchromatic metastatic-like cells. CAP treatment partially alleviated these changes, while VEM preserved hepatocyte morphology more effectively, though mild congestion and inflammation persisted. The CAP plus VEM group displayed near-normal hepatic architecture with minimal injury, reduced inflammatory activity, and negligible evidence of metastatic involvement (Figure 5).

Brain sections from untreated mice contained dense pigment aggregates and abnormal cellular clusters consistent with melanoma seeding. CAP reduced the extent of these deposits, whereas VEM showed a more substantial decline in metastatic features. Remarkably, the CAP and VEM group exhibited no detectable pigment accumulation or metastatic lesions, aside from mild edema in limited regions. These findings indicate robust protection against brain involvement (Figure 6).

Kidney tissue in untreated animals showed glomerular deformation, tubular dilation, hyperchromatic cells, and perivascular inflammatory infiltration. CAP and VEM each mitigated these alterations to varying degrees. The CAP plus VEM group showed largely preserved renal architecture. Only minimal inflammatory infiltration was observed. Nuclear atypia was markedly reduced, indicating substantial

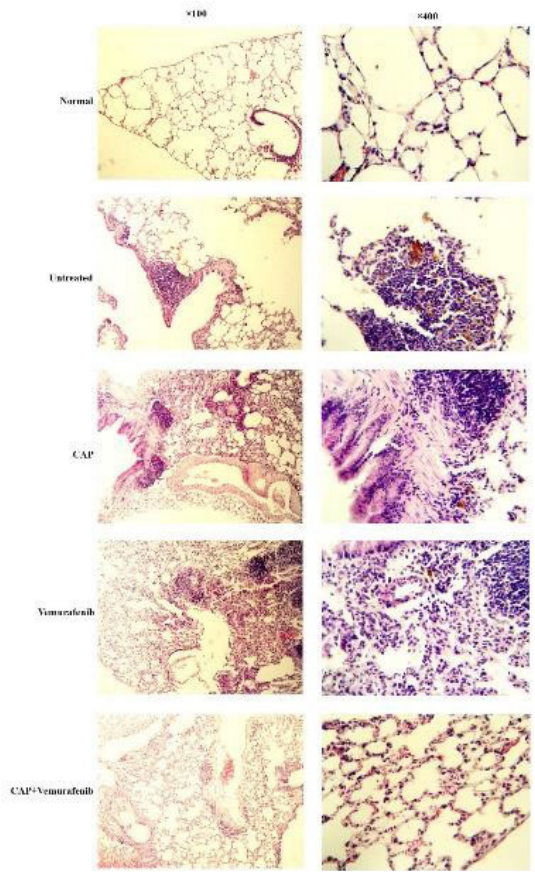

Figure 4. Histopathological analysis of lung tissues from C57BL/6 mice following CAP and vemurafenib treatment
Representative hematoxylin and eosin (H&E)–stained sections of lung tissues from normal, untreated, CAP-treated, Vemurafenib-treated, and CAP plus VEM groups are shown at low (×100) and high (×400) magnifications. Normal lung tissue displayed intact alveolar architecture with thin alveolar septa and clear air spaces. Conversely, lungs from untreated mice exhibited marked structural disruption characterized by inflammatory cell infiltration, septal thickening, and clusters of hyperchromatic cells suggestive of metastatic involvement. CAP or Vemurafenib monotherapy partially reduced these pathological alterations, with decreased inflammatory infiltration and improved preservation of alveolar structures. Notably, lung tissues from the CAP+Vemurafenib group exhibited largely preserved alveolar architecture with only minimal inflammatory cell infiltration. Moreover, the absence of prominent hyperchromatic or metastatic cell clusters in this group suggests a substantial protective effect against tumor-associated pulmonary alterations.
CAP: Cold atmospheric plasma; VEM: Vemurafenib

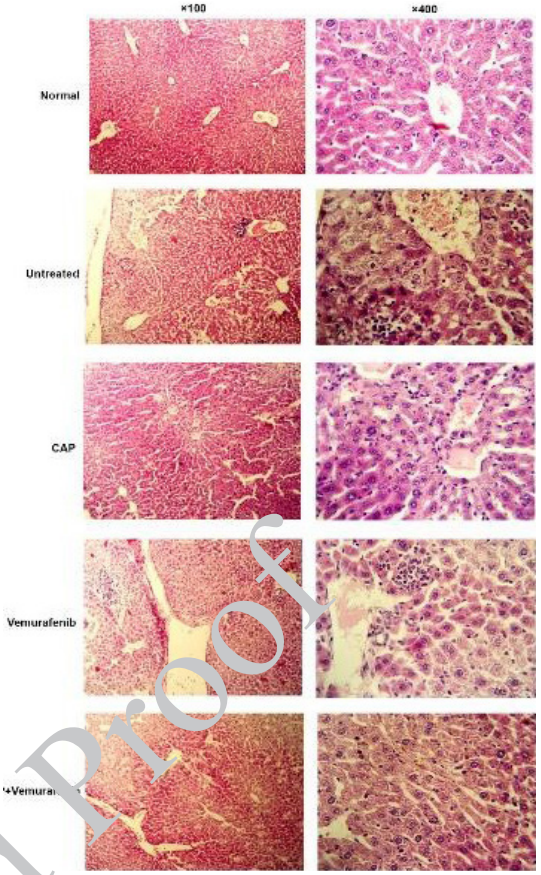

Figure 5. Histopathological evaluation of liver tissues from C57BL/6 mice following treatment with CAP and vemurafenib
Representative hematoxylin and eosin (H&E)–stained sections of liver tissues from normal, untreated, CAP-treated, Vemurafenib–treated, and CAP plus VEM groups are shown at low (×100) and high (×400) magnifications. Normal liver tissue displayed well-organized hepatic cords, intact hepatocytes with round nuclei, and preserved sinusoidal architecture. In contrast, liver sections from untreated mice exhibited marked structural alterations, including hepatocellular disorganization, sinusoidal dilation, and inflammatory cell infiltration. In addition, the presence of hyperchromatic cells suggested possible metastatic involvement. CAP treatment partially ameliorated these pathological changes, showing improved hepatocyte morphology and reduced inflammatory infiltration. Vemurafenib treatment also preserved hepatic architecture to some extent, although mild cellular alterations and congestion remained evident. Notably, the CAP plus VEM treatment resulted in substantial preservation of liver architecture. Reduced inflammatory infiltration and improved hepatocyte organization were observed in this group. These findings indicate a protective effect against tumor-associated hepatic injury.
CAP: Cold atmospheric plasma; VEM: Vemurafenib

protection against tumor-associated renal injury (Figure 7).

Analysis of MITF–P21 expression in vitro and in vivo after treatment with CAP and VEM

Quantitative real-time PCR analysis showed that all treatments markedly suppressed MITF expression in B16-F10 melanoma cells compared with untreated controls (P<0.0001; Figure 8A). A comparable pattern was observed for P21 expression, which was significantly dow-regulated after CAP and CAP plus VEM compared with the control group (P<0.0001; Figure 8B). Similar trends were observed in L929 fibroblasts; however, the magnitude of suppression was substantially lower than in melanoma cells. Correlation analysis revealed a strong positive association between MITF and P21 expression in B16-F10 cells (Spearman r=0.881, P=0.0072). A similarly positive, though slightly weaker, correlation was also observed in L929 fibroblasts (Spearman r=0.8571, P=0.01). These findings indicate coordinated regulation of the MITF–P21 axis at the cellular level (Supplementary Figure 1A and B). In contrast, qRT-PCR analysis of tumors from melanoma-bearing mice showed no significant changes in MITF or P21 expression after CAP, Vemurafenib, or CAP plus VEM compared with untreated controls (Figure 8C and D). *In vivo* correlation analysis showed a positive trend between MITF and P21 expression; however, this relationship did not reach statistical significance (Supplementary Figure 1C).

Suppression of metastatic markers MMP-2 and MMP-9 by CAP and VEM

Analysis of metastatic markers revealed a consistent inhibitory effect of CAP, VEM, and CAP plus VEM on *MMP-2* and *MMP-9* expression across the *in vitro* and *in vivo* experiments. As shown in Figure 9, in B16-F10 melanoma cells, all treatments significantly reduced *MMP-2* mRNA levels compared with untreated controls (P<0.0001), with CAP plus VEM exerting a greater suppressive effect than CAP alone (P=0.012). L929 fibroblasts similarly

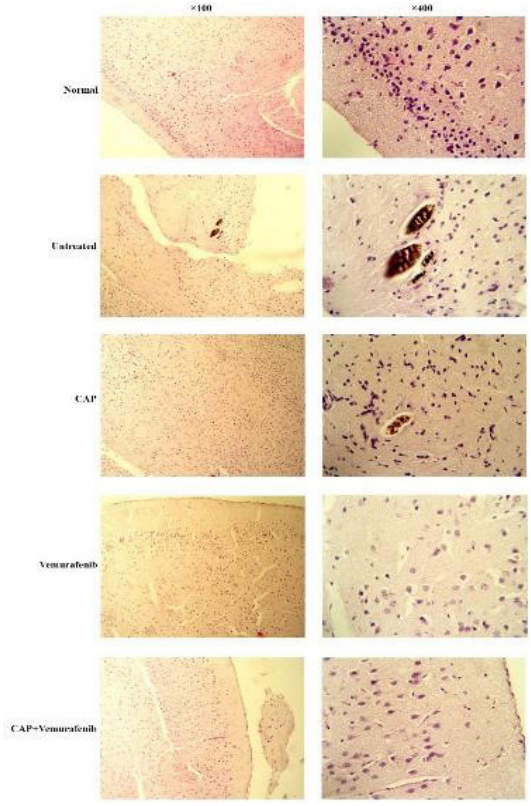

Figure 6. Histopathological evaluation of brain tissues from C57BL/6 mice following treatment with CAP and/or vemurafenib
Representative H&E-stained brain sections (×100 and ×400) from Normal, Untreated, CAP-treated, Vemurafenib-treated, and CAP+Vemurafenib groups are shown. Normal brain tissue exhibited intact cytoarchitecture with uniformly distributed neuronal and glial cells. Untreated melanoma-bearing mice displayed pronounced structural disruption, dense tumor cell infiltration, and localized necrotic changes. CAP treatment led to partial improvement, characterized by reduced cellular disorganization and milder infiltration. Vemurafenib-treated brains showed moderate preservation of tissue integrity with diminished tumor involvement. Notably, the CAP plus VEM resulted in the greatest structural preservation, demonstrating decreased tumor burden and improved overall tissue organization compared with the untreated group.
CAP: Cold atmospheric plasma; VEM: Vemurafenib

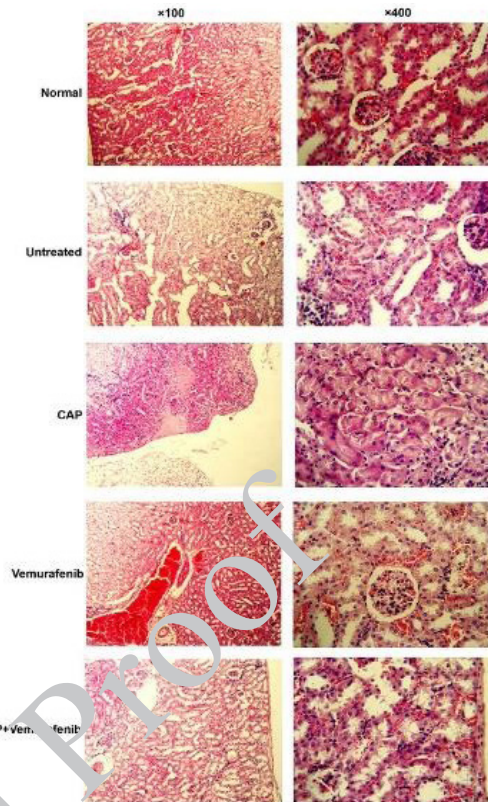

Figure 7. Histopathological evaluation of renal tissues from C57BL/6 mice following treatment with CAP and/or vemurafenib
Representative H&E-stained kidney sections (×100 and ×400) from Normal, Untreated, CAP-treated, Vemurafenib-treated, and CAP + Vemurafenib groups. Normal kidneys displayed intact glomeruli, preserved tubular architecture, and no signs of inflammation. The Untreated melanoma-bearing mice exhibited mild tubular degeneration, focal interstitial inflammation, and occasional glomerular alterations. CAP treatment resulted in moderate tubular dilation and patchy inflammatory infiltration. Vemurafenib-treated kidneys showed mild tubular vacuolization with limited inflammatory changes. Notably, the CAP plus VEM preserved overall renal architecture with minimal structural alterations, suggesting reduced treatment associated nephrotoxicity.
CAP: Cold atmospheric plasma; VEM: Vemurafenib

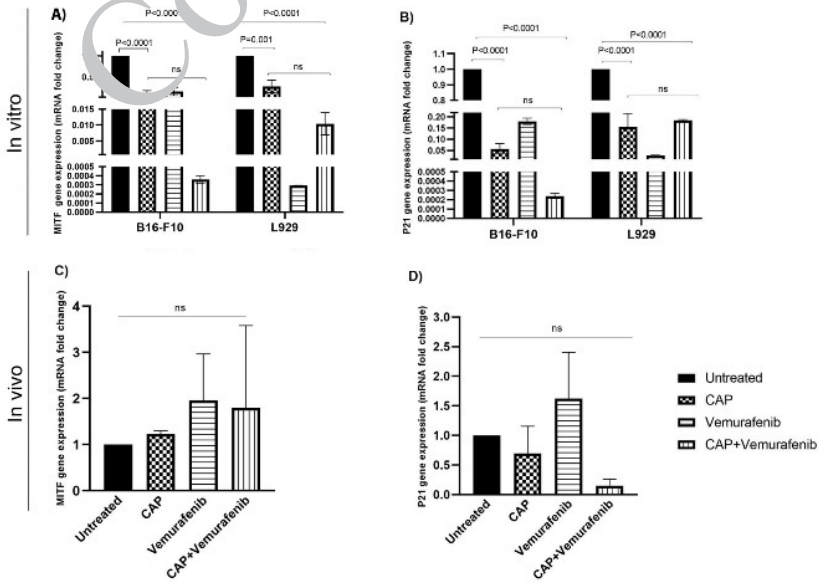

Figure 8. Comparative analysis of MITF and P21 gene expression *in vitro* and *in vivo* in C57BL/6 mice following treatment with CAP and/or vemurafenib
(A–B) Quantitative real-time PCR analysis of B16-F10 melanoma cells and L929 fibroblasts showing that CAP and CAP+Vemurafenib markedly dow-nregulated MITF (A) and P21 (B) expression compared with untreated controls, whereas Vemurafenib exerted a milder inhibitory effect. The magnitude of suppression was greater in B16-F10 melanoma cells than in L929 fibroblasts. (C-D) qRT-PCR analysis of tumor tissues from melanoma-bearing mice demonstrated that neither CAP, Vemurafenib, nor the CAP plus VEM significantly altered (C) MITF or (D) P21 expression relative to the untreated group. Data represent mean±SEM. ns, not significant.
CAP: Cold atmospheric plasma; VEM: Vemurafenib

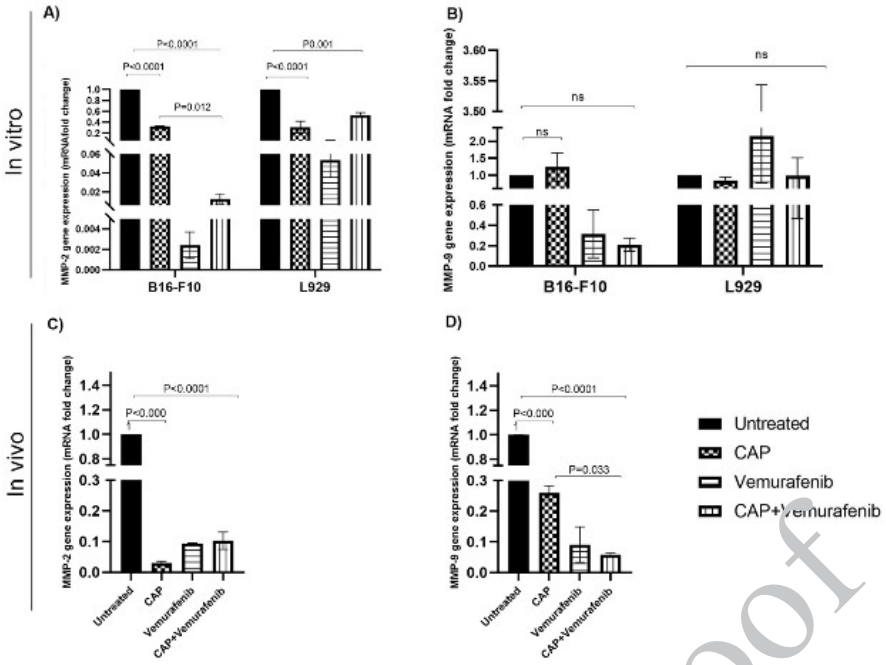

Figure 9. Comparative analysis of MMP-2 and MMP-9 gene expression *in vitro* and in tumor tissues of C57BL/6 mice following treatment with CAP and/or vemurafenib

(A–B) Quantitative real-time PCR analysis of B16-F10 melanoma cells and L929 fibroblasts showing that CAP and CAP plus VEM markedly reduced MMP-2 (A) expression in both cell types, while their effects on MMP-9 (B) were minimal and not statistically significant. (C–D) qRT-PCR analysis of tumor tissues from melanoma-bearing mice demonstrated that CAP, Vemurafenib, and CAP plus VEM significantly dow-nregulated both MMP-2 (C) and MMP-9 (D) expression compared with untreated controls. Data represent mean±SEM.

exhibited significant down-regulation of *MMP-2* following all treatments, although the CAP plus VEM group did not demonstrate an additional reduction relative to CAP. No significant alterations in *MMP-9* expression were detected in either cell line. Correlation analysis based on ΔCt values showed a positive but non-significant association between *MMP-2* and *MMP-9* expression in melanoma cells (Spearman r=0.71, P=ns). In contrast, no meaningful correlation was observed in fibroblasts. The *in vivo* qRT-PCR data corroborated the *in vitro* findings for *MMP-2*. Tumor tissues from CAP-treated mice exhibited a significant reduction in *MMP-2* expression relative to untreated tumors ($P<0.0001$). VEM and CAP plus VEM treatments similarly down-regulated *MMP-2*. However, CAP plus VEM did not show a significantly higher decrease than CAP alone. Unlike the cell-based results, all treatments significantly reduced *MMP-9* expression in tumor samples compared with untreated samples ($P<0.0001$), and CAP plus VEM resulted in greater suppression than CAP alone ($P=0.033$). Correlation analysis revealed a non-significant positive trend between *MMP-2* and *MMP-9* expression in tumor tissues (Spearman r=0.2857, $P>0.05$).

Discussion

Combination therapy is widely regarded as a promising strategy in cancer treatment. However, its success is not guaranteed and depends on the rational selection of therapeutic agents and their molecular targets. Therefore, selecting therapeutic strategies, treatment sequences, and optimal dosages is essential to avoid potential antagonistic interactions and maximize therapeutic benefit. In the context of CAP-based therapies, a deeper understanding of how plasma-generated reactive species interact with oncogenic signaling pathways, such as MITF-P21 signaling, and with metastasis-related regulators will be important for optimizing combination strategies (7, 8, 17-19).

In this context, the present study demonstrates that the CAP plus VEM enhances anti-tumor activity against melanoma in a mouse model. This combination resulted in reduction of cell proliferation, migration, clonogenic survival, and metastatic potential compared with either monotherapy. Integration of *in vitro* and *in vivo* data indicates that this multimodal strategy suppresses tumor progression more effectively than single-agent treatment, supporting the concept that CAP may serve as a supportive modality that enhances the therapeutic activity of VEM.

The clonogenic assay provides a robust measure of long-term cell proliferative capacity and therapeutic resistance. The assay showed that CAP suppresses the proliferative capacity of melanoma cells at both 7 and 14 days, indicating a sustained anti-tumor effect. While VEM alone initially reduced colony formation, partial recovery occurred after 14 days, consistent with the known development of adaptive resistance to BRAF inhibition (31-34). In contrast, CAP plus VEM maintained stronger, more persistent suppression of clonogenic growth. Normal fibroblasts showed recovery of colony formation, demonstrating partial selectivity for malignant cells. This difference likely reflects the elevated basal oxidative stress and altered redox balance in melanoma cells, rendering them more vulnerable to RONS produced by CAP. These findings are consistent with other studies supporting the potential of CAP as an adjuvant modality that may enhance the efficacy of cancer therapies (35-38).

Wound-healing assays revealed significant inhibition of B16-F10 cell migration by both CAP and VEM, with the strongest suppression observed with CAP plus VEM. Because migration is a critical early stage of metastasis, these findings suggest that the treatment may impair not only proliferative capacity but also metastatic behavior in melanoma cells. Previous studies have similarly reported

that CAP can reduce the migratory and invasive behavior of cancer cells (39-43). Histopathological analysis further confirmed these observations. Untreated tumors showed high cellular density and disorganized architecture typical of aggressive lesions. CAP alone produced moderate histological changes, whereas VEM treatment reduced cell density and induced partial necrosis. The CAP plus VEM combination exhibited the most prominent histopathological changes, including extensive necrotic areas, disrupted organization, decreased vascular congestion, and minimal metastatic foci, reflecting robust inhibition of tumor expansion *in vivo*.

MITF expression has been strongly implicated in melanoma progression, therapy resistance, and phenotypic plasticity (44-46). It has been reported to regulate cell-cycle progression, in part through transcriptional control of CDK inhibitors such as P21 (47, 48). At the molecular level, CAP markedly dow-nregulated MITF expression in melanoma cells, accompanied by reduced P21 levels. This pattern suggests that CAP disrupts the MITF–P21 regulatory axis, impairing lineage-specific transcriptional programs required for cell-cycle control and survival. The observed decline in P21 appears to result from MITF suppression followed by apoptotic degradation rather than from enhanced proliferation. Correlation analysis showed a positive association between MITF and P21 expression in melanoma cells but not in normal fibroblasts, highlighting the melanoma-specific dependency of this regulatory pathway.

MMPs, particularly MMP-2 and MMP-9, play critical roles in melanoma invasion and metastasis by degrading basement membrane components (25, 49-51). CAP plus VEM significantly reduced *MMP-2* expression *in vitro* and dow-regulated both *MMP-2* and *MMP-9 in vivo*, indicating potent inhibition of metastatic remodeling processes. These molecular trends corresponded with the observed histopathological suppression of invasion. Similarly, CAP has been associated with reduced expression of metastasis-related proteases (43, 52, 53). But this effect is not evaluated in CAP plus VEM.

Collectively, these data indicate that CAP enhances VEM efficacy by disrupting proliferative and metastatic signaling, suggesting its potential for integration into multimodal melanoma therapy. Future studies should explore the mechanistic interplay among CAP-generated reactive species, the BRAF/MAPK pathway, and immune modulation within the tumor microenvironment and evaluate treatment selectivity in more physiologically relevant models, such as co-culture systems and primary melanocytes.

Conclusion

This study shows that CAP plus VEM produces a stronger anti-tumor effect against melanoma than either treatment alone, in both *in vitro* and *in vivo* settings. The CAP plus VEM markedly reduced cell proliferation, migration, clonogenic survival, and metastatic spread, while inducing clear histopathological evidence of tumor necrosis and decreased cellularity. At the molecular level, suppression of MITF–P21 (*in vitro*) and significant dow-regulation of MMP-2 and MMP-9 (*in vivo*) indicate inhibition of pathways involved in tumor growth and metastasis. Although these findings demonstrate promising therapeutic potential, they are limited to *in vitro* and murine models; therefore, further preclinical investigations and well-designed clinical trials are required to evaluate the safety and clinical applicability of this strategy in patients with melanoma.

Acknowledgment

The authors would like to thank Mazandaran University of Medical Sciences for its support.

Ethics Approval and Consent to Participate

The protocol of this study was approved by the Research Ethics Committee of Mazandaran University of Medical Sciences, IR.MAZUMS.AEC.1402.079.

Availability of Data and Materials

The data that support the findings of this study are available from the corresponding author upon reasonable request.

Funding

This research was funded by the Research and Technology Deputy of Mazandaran University of Medical Sciences (grant number 15127) and the National Institute for Medical Research Development (NIMAD) (grant number 4031031).

Authors' Contributions

Z Y and AR designed the experiments. Z Y performed the experiments and collected the data. Z Y, M M, S F, A M, F M, and Z R contributed to the experimental procedures and methodology. Z Y conducted the formal analysis and data curation. Z Y, S A, and M G contributed to the investigation. AR and FS provided resources. Z Y and A R interpreted the results and discussed the study strategy. A R supervised, directed, and managed the project and secured funding. Z Y prepared the original draft of the manuscript, and A R reviewed and edited it. All authors approved the final version of the manuscript for publication.

Conflicts of Interest

The authors declare that they have no competing interests.

Declaration

During the preparation of this manuscript, the authors used ChatGPT (OpenAI, San Francisco, CA, USA) to assist with language editing and to improve the clarity and readability of the text. The tool was also used to help draft the schematic illustration in the graphical abstract, based on the authors' conceptual design and scientific interpretation. The artificial intelligence tool was not used to generate scientific data, perform data analysis, or independently interpret the results. All experimental data, analyses, interpretations, and conclusions were developed and verified by the authors, who take full responsibility for the accuracy and integrity of the work.

References

1. Salah S, Kerob D, Ezzedine K, Khurana P, Balan D, Passeron T. Analysis of global skin cancer epidemiology in 2022 and correlation with dermatologist density. J Eur Acad Dermatol Venereol 2025; 40:e221.

2. Galliker NA, Murer C, Kamarashev J, Dummer R, Goldinger SM. Clinical observation of panniculitis in two patients with BRAF-mutated metastatic melanoma treated with a combination of a BRAF inhibitor and a MEK inhibitor. Eur J Dermatol 2015; 25:177–180.

3. Dugan MM, Perez MC, Karapetyan L, Zager JS. Combination atezolizumab, cobimetinib, and vemurafenib as a treatment option in BRAF V600 mutation–positive melanoma: Patient selection and

perspectives. Cancer Manag Res 2024:933–939.
4. Luke JJ, Hodi FS. Ipilimumab, vemurafenib, dabrafenib, and trametinib: Synergistic competitors in the clinical management of BRAF mutant malignant melanoma. Oncologist 2013; 18:717–725.
5. Li H, Wang Y, Su R, Jia Y, Lai X, Su H, *et al.* Dimethyl fumarate combined with vemurafenib enhances anti-melanoma efficacy via inhibiting the hippo/YAP, NRF2-ARE, and AKT/mTOR/ERK pathways in A375 melanoma cells. Front Oncol 2022; 12:794216.
6. Mahmoudi G, Ehteshaminia Y, Kokhaei P, Jalali SF, Jadidi-Niaragh F, Pagheh AS, *et al.* Enhancement of targeted therapy in combination with metformin on human breast cancer cell lines. Cell Commun. Signal 2024; 22:10.
7. Mokhtari RB, Homayouni TS, Baluch N, Morgatskaya E, Kumar S, Das B, *et al.* Combination therapy in combating cancer. Oncotarget 2017; 8:38022.
8. Medina TM, Lewis KD. The evolution of combined molecular targeted therapies to advance the therapeutic efficacy in melanoma: A highlight of vemurafenib and cobimetinib. Onco Targets Ther 2016:3739–3752.
9. Larkin J, Ascierto PA, Dréno B, Atkinson V, Liszkay G, Maio M, *et al.* Combined vemurafenib and cobimetinib in BRAF-mutated melanoma. N Engl J Med 2014; 371:1867–1876.
10. Ribas A, Gonzalez R, Pavlick A, Hamid O, Gajewski TF, Daud A, *et al.* Combination of vemurafenib and cobimetinib in patients with advanced BRAFV600-mutated melanoma: A phase 1b study. Lancet Oncol 2014; 15:954–965.
11. Niehr F, von Euw E, Attar N, Guo D, Matsunaga D, Sazegar H, *et al.* Combination therapy with vemurafenib (PLX4032/RG7204) and metformin in melanoma cell lines with distinct driver mutations. J Transl Med 2011; 9:76.
12. Faramarzi F, Zafari P, Alimohammadi M, Moonesi M, Rafiei A, Bekeschus S. Cold physical plasma in cancer therapy: Mechanisms, signaling, and immunity. Oxid Med Cell Longev 2021; 2021:9916796.
13. Yazdani Z, Pasandi MS, Golpour M, Eslami M, Rafiei A. Effect of cold atmospheric plasma on changing of biomolecular structures involved in apoptosis pathways of melanoma cancer. Skin Res Technol 2024; 30:e13544.
14. Golpour M, Asgarian-Omran H, Akhavan-Niaki H, Alimohammadi M, Alizadeh-Forutan M, Sohbatzadeh F, *et al.* Cold plasma treatment of patient-derived chronic lymphocytic B-cell leukemia enhances cytotoxic T-cell proliferation. Plasma Process Polym 2024; 21:2400008.
15. Gkantaras A, Kotzamanidis C, Kyriakidis K, Farmaki E, Makedou K, Tzimagiorgis G, *et al.* Multi-cohort transcriptomic profiling of medical gas plasma-treated cancers reveals the role of immunogenic cell death. Cancers 2024; 16:2186.
16. Bekeschus S, Singer D, Ratnayake G, Ruhnau K, Ostrikov K, Thompson EW. Rationales of cold plasma jet therapy in skin cancer. Exp Dermatol 2025; 34:e70063.
17. Yu L, Berner J, Martinet A, Freund E, Singer D, von Woedtke T, *et al.* Gas plasma combination therapies—promises from preclinical oncology research. Antioxidants 2025; 14:1055.
18. Yazdani Z, Mehrabanjoubani P, Rafiei A, Biparva P, Kardan M. Combined effect of cold atmospheric plasma and curcumin in melanoma cancer. Biomed Res Int 2021; 2021:1969863.
19. Jawaid P, Rehman MU, Zhao QL, Takeda K, Ishikawa K, Hori M, *et al.* Helium-based cold atmospheric plasma-induced reactive oxygen species-mediated apoptotic pathway attenuated by platinum nanoparticles. J Cell Mol Med 2016; 20:1737–1748.
20. Tudrej KB, Czepielewska E, Kozłowska-Wojciechowska M. SOX10-MITF pathway activity in melanoma cells. Arch Medl Sci 2017; 13:1493–1503.
21. Cronin JC, Watkins-Chow DE, Incao A, Hasskamp JH, Schönewolf N, Aoude LG, *et al.* SOX10 ablation arrests cell cycle, induces senescence, and suppresses melanomagenesis. Cancer Res 2013; 73:5709–5718.
22. Shakhova O, Zingg D, Schaefer SM, Hari L, Civenni G, Blunschi J, *et al.* Sox10 promotes the formation and maintenance of giant congenital naevi and melanoma. Nat Cell Biol 2012; 14:882–890.
23. Birkedal-Hansen H. Proteolytic remodeling of extracellular matrix. Curr Opin Cell Biol 1995; 7:728–735.
24. Shapiro SD. Matrix metalloproteinase degradation of extracellular matrix: biological consequences. Curr Opin Cell Biol 1998; 10:602–608.
25. Redondo P, Lloret P, Idoate M, Inoges S. Expression and serum levels of MMP-2 and MMP-9 during human melanoma progression. Clin Exp Dermatol 2005; 30:541–545.
26. Zafari P, Yadani Z, Akhavan-Niaki H, Rafiei A. Effect of cold atmospheric plasma on gene expression and methylation of genes involved in colorectal cancer. J Mazandaran Univ Med Sci 2022.
27. Alimohammadi M, Golpour M, Sohbatzadeh F, Hadavi S, Bekeschus S, Niaki HA, *et al.* Cold atmospheric plasma is a potent tool to improve chemotherapy in melanoma *in vitro* and *in vivo*. Biomolecules 2020; 10:1011.
28. Franken NA, Rodermond HM, Stap J, Haveman J, Van Bree C. Clonogenic assay of cells *in vitro*. Nat Protoc 2006; 1:2315–2319.
29. Fattahi S, Amirbozorgi G, Lotfi M, Amini Navaei B, Kavoosian S, Asouri M, *et al.* Development of a universal taqman probe for mRNA gene expression analysis. Iran J Sci Technol Trans A: Sci 2018; 42:363–370.
30. Fattahi S, Pilehchian Langroudi M, Samadani AA, Nikbakhsh N, Asouri M, Akhavan-Niaki H. Application of unique sequence index (USI) barcode in gene expression profiling in gastric adenocarcinoma. J Cell Commun Signaling 2017; 11:97–104.
31. Manzano RL, Reyos A, Bugés C, de los Llanos Gil M, Vila L, Martínez-Balibrea E, *et al.* Resistant mechanisms to BRAF inhibitors in melanoma. Ann Transl Med 2016; 4:237.
32. Proietti I, Skroza N, Bernardini N, Tolino E, Balduzzi V, Marchesiello A, *et al.* Mechanisms of acquired BRAF inhibitor resistance in melanoma: a systematic review. Cancers 2020; 12:2501.
33. Hernandez-Davies JE, Tran TQ, Reid MA, Rosales KR, Lowman XH, Pan M, *et al.* Vemurafenib resistance reprograms melanoma cells towards glutamine dependence. J Transl Med 2015; 13:210.
34. Tabolacci C, Cordella M, Mariotti S, Rossi S, Senatore C, Lintas C, *et al.* Melanoma cell resistance to vemurafenib modifies intercellular communication signals. Biomedicines 2021; 9:79.
35. Yan C, Zhao L, Zhang X, Chu Z, Zhou T, Zhang Y, *et al.* Cold atmospheric plasma sensitizes melanoma cells to targeted therapy agents *in vitro*. J Biophotonics 2024; 17:e202300356.
36. Kniazeva V, Tzerkovsky D, Baysal Ö, Kornev A, Roslyakov E, Kostevitch S. Adjuvant composite cold atmospheric plasma therapy increases antitumoral effect of doxorubicin hydrochloride. Front Oncol 2023; 13:1171042.
37. Park J, Jang Y-S, Choi J-H, Ryu M, Kim G-C, Byun J-H, *et al.* Anticancer efficacy of nonthermal plasma therapy combined with PD-L1 antibody conjugated gold nanoparticles on oral squamous cell carcinoma. Appl Sci 2021; 11:4559.
38. Daeschlein G, Hillmann A, Gümbel D, Sicher C, von Podewils S, Stope MB, *et al.* Enhanced anticancer efficacy by drug chemotherapy and cold atmospheric plasma against melanoma and glioblastoma cell lines *in vitro*. IEEE Trans Radiat Plasma Med Sci 2018; 2:153–159.
39. Pavlović O, Lazarević M, Jakovljević A, Škoro N, Puač N, Mojsilović S, *et al.* Antitumor potential of different treatment approaches using cold atmospheric pressure plasma on oral squamous cell carcinoma models: *In vitro* study. Biomedicines 2025; 13:443.
40. Özdemir GD, Ercan UK, Karaman O, Oltulu F. Effect of direct plasma treatment and plasma-treated liquid on cutaneous squamous cell carcinoma: A proof-of-concept study. Plasma Process Polym 2023; 20:e2200246.
41. Wang M, Holmes B, Cheng X, Zhu W, Keidar M, Zhang LG. Cold atmospheric plasma for selectively ablating metastatic breast cancer cells. PLoS One 2013; 8:e73741.
42. Wang Y, Eggers B, Abazid A, Erb HH, Stope MB. Non-invasive physical plasma as an oncological therapy option: modulation of cancer cell growth, motility, and metabolism without induction of cancer resistance factors. Cancers 2025; 17:3517.

43. Chang JW, Kang SU, Shin YS, Kim KI, Seo SJ, Yang SS, *et al.* Non-thermal atmospheric pressure plasma inhibits thyroid papillary cancer cell invasion via cytoskeletal modulation, altered MMP-2/-9/uPA activity. PLoS One 2014; 9:e92198.
44. Lai X, Luan C, Zhang Z, Wessely A, Heppt MV, Berking C, *et al.* SOX10, MITF, and microRNAs: Decoding their interplay in regulating melanoma plasticity. Int J Cancer 2025;157: 1277-1293.
45. Kaufman CK. Specific SOX10 enhancer elements modulate phenotype plasticity and drug resistance in melanoma. BioRxiv 2024; 2024.
46. Lavelle TJ, Alver TN, Heintz K-M, Wernhoff P, Nygaard V, Nakken S, *et al.* Dysregulation of MITF leads to transformation in MC1R-defective melanocytes. Cancers 2020; 12:1719.
47. Liu F, Singh A, Yang Z, Garcia A, Kong Y, Meyskens Jr FL. MiTF links Erk1/2 kinase and p21CIP1/WAF1 activation after UVC radiation in normal human melanocytes and melanoma cells. Mol Cancer 2010; 9:214.
48. Šestáková B, Ondrušová L, Vachtenheim J. Cell cycle inhibitor p21/WAF1/CIP1 as a cofactor of MITF expression in melanoma cells. Pigment Cell Melanoma Res 2010; 23:238–251.
49. Pereira AMM, Strasberg-Rieber M, Rieber M. Invasion-associated MMP-2 and MMP-9 are up-regulated intracellularly in concert with apoptosis linked to melanoma cell detachment. Clin Exp Metastasis 2005; 22:285–295.
50. Hofmann UB, Westphal JR, van Muijen GN, Ruiter DJ. Matrix metalloproteinases in human melanoma. J Invest Dermatol 2000; 115:337–344.
51. Zeng Z-S, Cohen AM, Guillem JG. Loss of basement membrane type IV collagen is associated with increased expression of metalloproteinases 2 and 9 (MMP-2 and MMP-9) during human colorectal tumorigenesis. Carcinogenesis 1999; 20:749–755.
52. Soulat A, Mohsenpour T, Roshangar L. Dual-jet transition cold atmospheric plasma suppresses colon cancer stem cells via matrix metalloproteinase regulation. Cancer Treat Res Commun 2026:101096.
53. Liu JR, Gao LG, Wu YM, Xu GM, Ma Y, Hao Y, *et al.* Low-temperature plasma-activated medium inhibited invasion and metastasis of melanoma cells via suppressing the Wnt/β-catenin pathway. Plasma Process Polym 2020; 17:1900060.